Multi-physical modelling of reverse electrodialysis

L. Gurreri[a], G. Battaglia[b], A. Tamburini[a]*, A. Cipollina[a], G. Micale[a], M. Ciofalo[a]

[a]Dipartimento dell'Innovazione Industriale e Digitale (DIID), Università degli Studi di Palermo (UNIPA) – viale delle Scienze Ed.6, 90128 Palermo, Italy.

[b]Dipartimento di Ingegneria Civile, Ambientale, Aerospaziale, dei Materiali (DICAM), Università degli Studi di Palermo (UNIPA) – viale delle Scienze Ed. 8, 90128 Palermo, Italy.

*email: alessandro.tamburini@unipa.it

Abstract

Reverse electrodialysis (RED) is an electrochemical membrane process that directly converts the energy associated with the concentration difference between two salt solutions into electrical energy by means of a selective controlled mixing. The physics of RED involves the interaction of several phenomena of different nature and space-time scales. Therefore, mathematical modelling and numerical simulation tools are crucial for performance prediction. In this work, a multi-physical modelling approach for the simulation of RED units was developed. A periodic portion of a single cell pair was simulated in two dimensions. Fluid dynamics was simulated by the Navier-Stokes and continuity equations, and ion transfer by the Nernst–Planck approach along with the local electroneutrality condition. The Donnan exclusion theory was implemented in order to simulate interfacial phenomena. A sensitivity analysis of the process performance was carried out. Different membrane/channel geometrical configurations were investigated, including flat membranes, either with or without non-conductive spacers, and profiled membranes. The influence of feeds concentration/velocity was also evaluated. Results confirmed that, with respect to the ideal case of plane (empty) channels and planar membranes, non-conductive spacers always reduce the power

1

produced, while profiled membranes may or may not perform better, depending on stack features and operating conditions.

Keywords: Reverse electrodialysis, multi-physical model, finite element method, power density, profiled membranes.

1   Introduction

1.1   Principle of RED

Different technologies have been proposed in order to exploit the energy of salinity gradients [1–4]. Reverse electrodialysis (RED) was the first concept proposed [5] and appears to be the most promising, as it exhibits the highest power density [6] and can become competitive with the other renewable energy processes thanks to process optimization [7] and membrane cost abatement.

The basic repetitive unit of a RED stack (Figure 1) comprises an anion exchange membrane (AEM), a concentrate compartment (CONC), a cation exchange membrane (CEM), and a dilute compartment (DIL). This repetitive unit is usually denoted as a *cell pair*, although some may prefer the term *cell*. Throughout this paper, the notation "cell pair" will be adopted.
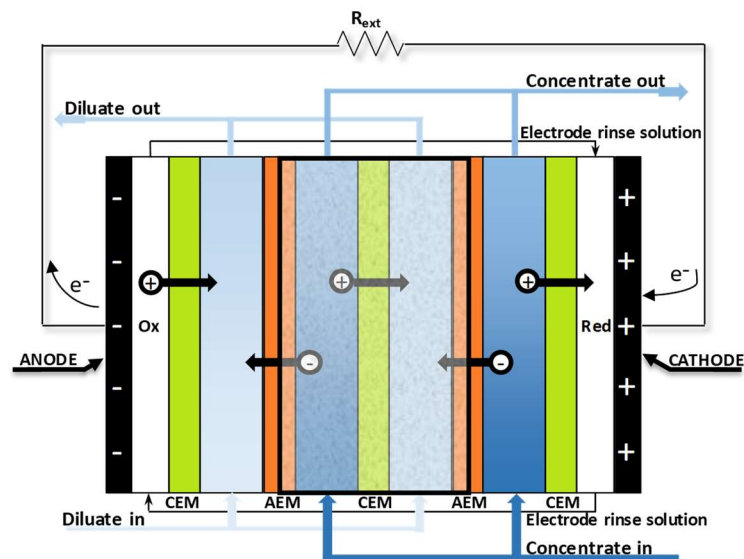

Figure 1. Sketch of a reverse electrodialysis stack.

Flat AEMs and CEMs are usually separated by net spacers, but the process performance may be enhanced by the use of self-supporting profiled membranes [8].

Due to the electrochemical equilibrium, an ion exchange membrane (IEM) immersed between two solutions at different concentrations is subject to a voltage difference (Donnan exclusion) [9], and the sum of all the membrane potentials of a stack is the open circuit voltage (OCV). Under closed circuit conditions, redox reactions arise due to the voltage difference at the electrodes, thus providing an electrical current to the load. At the same time, a selective ionic transport takes place within the stack from each concentrated channel to the adjacent dilute channels.

1.2 Critical aspects

The theoretical (maximum) electromotive force, or OCV, is proportional to the logarithm of the ratio between the ion activities in the two solutions. However, the use of highly concentrated solutions may imply a significant reduction of the IEMs ability to allow the passage of a single ionic species (permselectivity) [10,11]. The voltage over the external load can be expressed as OCV less the voltage loss due to the internal resistance of the stack, which takes into account different phenomena.

Ohmic losses (η_Ω) are mainly due to the resistance of the dilute channel when low concentration solutions, e.g. river water, are used [12–14]. Stacks with net spacers made by non-conductive material may cause an increase of η_Ω by more than 50% [10,12–15], while stacks with profiled membranes perform better [8,16]. Very recently, stacks equipped with chevron profiled membranes exhibited higher net power density values with respect to other stacks with net spacers or pillar profiled membranes [17].

The ion transport across IEMs causes a streamwise concentration variation in the bulk of the solution and a concentration variation perpendicular to the membranes within the diffusion boundary layers. These concentration non-uniformities give rise to further voltage drops, referred to as non-Ohmic losses ($\eta_{\Delta c}$ and η_{BL}) [18]. $\eta_{\Delta c}$ is determined by the ion mass balance within the

3

channels. In stacks fed by river water - seawater solutions, under conditions of maximum net power density, $\eta_{\Delta c}$ is a relevant contribution to the total voltage loss [10,14,16].

Concentration polarisation phenomena cause a change of the Donnan potential with consequent reduction of the actual voltage over the membrane [19]. With the standard river water – seawater solutions η_{BL} may be significant [13,14,16,20]; however, at the flow rates allowing the maximum net power density it is usually lower than the other contributions to the overall voltage drop when using spacers [10,14,16], although Vermaas *et al.* [16] found it to be larger than $\eta_{\Delta c}$ and only slightly lower than η_{Ω} when using profiled membranes (mixing not favoured). As the feeds concentrations increase, concentration variations are relatively lower and thus non-Ohmic effects decrease [10,21].

The pumping power consumption may considerably reduce the actual power. Net spacers may increase by several times hydraulic friction in the channel with respect to the ideal case of a spacer-less channel [8,21,22], while simple profiled membranes may be preferable [8,16,23]. Several experimental data showed pressure drop within the manifolds comparable or higher than those distributed in the channels [8,16,24–26]. However, pressure drop within the manifolds can be significantly reduced by adopting a suitable geometry [8,27].

1.3   State of the art of the small scale simulation

In several studies, e.g. Veerman *et al.* 2011 [28], RED stacks have been simulated taking no account of concentration polarization effects, which amounts to assuming $\eta_{BL} = 0$. On the other hand, in previous papers we used CFD to simulate spacer-filled and profiled-membrane channels for RED applications [21–23,29]. Navier–Stokes and continuity equations and a transport equation for a binary electrolyte (NaCl) were solved by using the 3-D CFD code *Ansys CFX™* [30]. Synthetic parameters (dimensionless numbers) quantifying pressure drop and mass transfer, such as Sherwood numbers and friction coefficients, were calculated. These CFD results can be combined with a large-scale 1-D model of a RED stack to provide realistic performance predictions [31]. A

4

similar simulation approach had been devised by Pawlowski *et al*. [32] on the basis of the open-source *Open-FOAM* software [33]. Models based on a diffusion-convection approach were also developed by other authors, investigating some specific aspects concerning RED units. For example, Kim *et al*. [34] studied a module with channels in serial configuration, Weiner *et al*. [35] proposed to improve the stack performance by blending the low salinity feed with a higher salinity stream before the stack entrance, Moya [36] evaluated the thickness of the diffusion boundary layer and the optimal load resistance.

If a knowledge of the spatial distribution of the electrical potential is desired, then a convection-diffusion equation is not sufficient, but ionic migration must be taken into account. The Nernst–Planck equation is commonly adopted along with the local electroneutrality condition. Several works were carried out by following this approach for electrodialysis (ED)/RED systems. Among these works, Jeong *et al*. [37] proposed a FEM model of RED implemented in *COMSOL™* [38]. A cell pair of 0.4 m long spacer-less channels was simulated in 2-D (axial + cross-membrane); membranes were not included in the computational domain, but were modelled by imposing boundary conditions. The maximum net power density was obtained by choosing a channel thickness of ~150 μm and a fluid velocity of ~4 cm/s. Zourmand *et al*. [39] developed a similar *COMSOL*-based model for ED devices. Membranes were simulated as domains with Ohmic behaviour, i.e. by neglecting the effect of concentration variations. Tadimeti *et al*. [40] extended the model in order to investigate the effect of obstacles (spacer/corrugations), and validated it against experimental data [41]. Tedesco *et al*. [42] conducted 2-D simulations of transport phenomena in ED/RED systems. The computational domain consisted of two empty half channels and one membrane, i.e. a symmetric behaviour was assumed for the two ionic species of a 1:1 salt and for the two membranes. The effect of co-ion transport on the process performance was assessed, and permselectivity and electrical resistance of membranes were predicted as functions of the fixed charge density and of the position along the channel.

1.4 Aim of the present work

From the (brief, but sufficiently complete) review conducted in the previous section, it appears clear that the modelling of electro-membrane processes is a very complex task. The mathematical models proposed in the literature are based on simplifying assumptions on (i) the geometry of the domain simulated and (ii) the physics of the phenomena involved.

The aim of this work was to develop a relatively complete modelling tool for RED systems, able physically to describe the transport phenomena within the cell pair and to compare the performance of RED stacks characterized by different membrane/channel configurations. The model simulates simultaneously fluid dynamics and ionic transport in two dimensions within a periodic geometrical unit of the cell pair. The only feature of the stack that the model does not simulate is the stack length with the related axial voltage drop ($\eta_{\Delta c}$). Electrochemical mass transport is simulated by the Nernst–Planck equation along with the local electroneutrality condition, and double layer phenomena are simulated by the Donnan exclusion theory. Membranes were explicitly simulated as parts of the computational domain, and the 2-D spatial distribution of concentration, current density and electrical potential is predicted within the whole cell pair. Various membrane/channel geometrical configurations were studied and the influence of concentration and velocity of feed solutions was assessed. The electrical power delivered by a stack to an external load was computed, thus giving important information for the optimization of stack and operating conditions.

2   Physical and numerical modelling

2.1   Simulation approach

The geometrical domain of a RED cell pair was simulated in 2-D (axial + cross-membrane). As an example, Figure 2 shows a typical profiled-membrane configuration among those investigated.
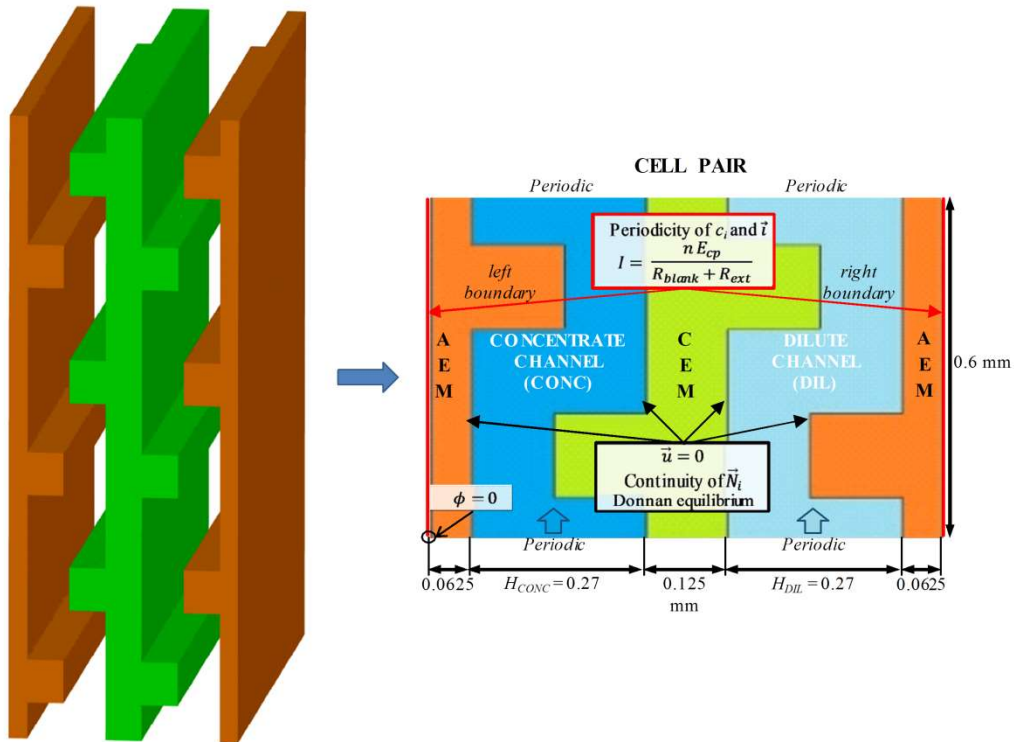
Figure 2. Typical configuration (staggered rectangular profiles). Left: hypothetical three-dimensional geometry; right: two-dimensional computational domain (unit cell) and boundary conditions.

The model was implemented in the FEM commercial software *COMSOL Multiphysics*[®] [38]. To the best of our knowledge, this is one of the very few codes allowing a complete physical description of the coupled physical phenomena (electrochemistry, fluid dynamics, diffusion) occurring in a RED unit. The choice of adopting a two-dimensional model of the cell pair was, to a large extent, a forced consequence of this option; in fact, the effort that this code would require for a complete three-dimensional simulation is overwhelming. Of course, a price has to be paid for this limitation, in that the real geometry of a profiled membrane or of a net spacer could not be described in two dimensions only, and only drastically simplified geometries such as that in Figure 2 had to be selected.

However, most of the physical aspects of the real RED process were well preserved in the simulations, including the influence of membrane properties, solution concentrations, residence

times and coupling with an external load. Phenomena which are less effectively modelled as two-dimensional include those related with the spatial current density distribution and the convective flow field; however, the use of judicious corrections can deal also with these phenomena to a satisfactory accuracy. The most serious shortcoming of a 2-D model is that obstacles spanning the whole channel thickness cannot be simulated; therefore, spacers and profiled membranes had to be described by non-obstructing shapes which occupy only a fraction of the thickness of each channel but maintain some of the features of real 3-D obstacles, such as their porosity. Also previous studies of RED or ED processes have met with similar limitations and have adopted 2-D geometries only partly representative of real-world configurations [37,39,40,42] [Jeong, Zourmand, Tadimeti, Tedesco].

Electrode compartments were not explicitly simulated, but their resistance (blank resistance, R_{blank}) was taken into account as shown below. By considering the equivalent electrical circuit of the system (Figure 3), the electrical quantities relevant to a stack of n cell pairs and a membrane projected area S_{stack} could be computed. The values of the main parameters adopted in the simulations are summarized in Table 1.
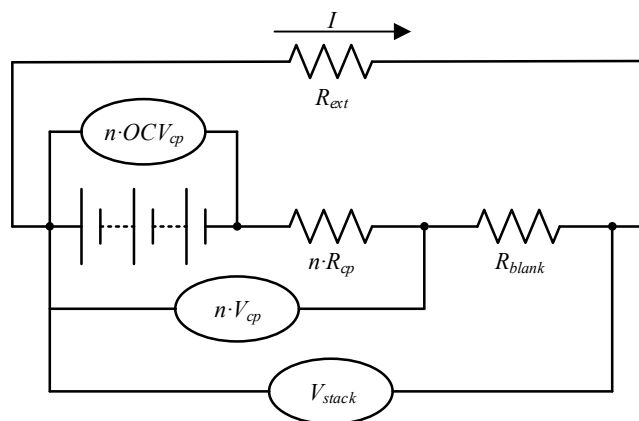

Figure 3. Equivalent electrical circuit.

Table 1 - Values of the main parameters adopted in the simulations.

		Value	Unit
Domain length		0.6	mm
Obstacle side length		0.15	mm
Base thickness			
	CEM	0.125	mm
	AEM	0.125	mm
	Channel	0.270	mm
Concentrations			
	Concentrated solution	4	M
	Dilute solution	0.005, 0.01, 0.05, 0.1, 0.5	M
	AEM fix charges	4.267	M
	CEM fix charges	4.833	M
Superficial velocity in both channels		0.3-5	cm/s
Temperature		20	°C

2.2 Governing equations

Continuity and momentum transport (Navier-Stokes) equations for a Newtonian, constant property, fluid are:

$$\nabla \cdot \mathbf{u} = 0 \tag{1}$$

$$\rho \frac{\partial \mathbf{u}}{\partial t} + \rho \mathbf{u} \nabla \mathbf{u} = -\nabla p + \mu \nabla^2 \mathbf{u} + \mathbf{P} \tag{2}$$

where ρ is density, t is time, $\mathbf{u}$ is velocity vector, p is pressure, μ is dynamic viscosity and $\mathbf{P}$ is a source term used to model periodicity (see following section 2.3).

Mass transport of ionic species is described in the Nernst-Planck approach by the following equation (diffusion + migration + convection):

$$\mathbf{N}_i = -D_i \nabla c_i - z_i m F c_i \nabla \phi + \mathbf{u} c_i \tag{3}$$

where the subscript i indicates the ionic species, D_i is the diffusivity, c_i is the ion concentration, z_i is the valence, m is the mobility, F is Faraday's constant, ϕ is the electrical potential and $\mathbf{N}_i$ is the total flux of species i. The mass balance in the absence of reactions of production/consumption is:

$$\frac{\partial c_i}{\partial t} + \nabla \cdot \mathbf{N}_i = S_i \tag{4}$$

where S_i is a source term used to model periodicity (see following section 2.3). The local electroneutrality condition was assumed:

$$\sum z_i c_i = 0 \tag{5}$$

In the membrane domains, also the concentration of fixed charges was included in the terms c_i. The current density is given by:

$$\mathbf{i} = F \sum_i z_i \mathbf{N}_i \tag{6}$$

Multiplication of Eq. (4) by $z_i F$ and summation over the species taking Eqs. (5) and (6) into account yields the conservation of charge:

$$\nabla \cdot \mathbf{i} = 0 \tag{7}$$

With reference to the equivalent electrical circuit in Figure 3, by linking the distributed values of current density and electrical potential with the quantities relevant to the external circuit, and adding Ohm's law for the external circuit, one can obtain the boundary conditions for current density and electrical potential. The length-average of voltage and current density over one cell pair are calculated at the boundaries of the computational domain in Figure 2 (arbitrarily located at mid-AEM)

$$\langle i \rangle = \frac{1}{l} \int i \, dl \tag{8}$$

$$\langle\phi\rangle = \frac{1}{l}\int \phi \, dl \tag{9}$$

where l denotes the length of the 2-D domain simulated. The voltage over the cell pair is calculated as the difference between the average values of ϕ at the external boundaries:

$$V_{cp} = \langle\phi_{right}\rangle - \langle\phi_{left}\rangle \tag{10}$$

In the following, the dimensions of the stack in the axial and lateral directions will be denoted by L_{stack} and W_{stack}, respectively. The projected area of the stack will thus be $S_{stack} = L_{stack} \cdot W_{stack}$. The average voltage and the average current density over the cell pair are supposed to be uniform along the flow direction (i.e. the axial voltage drop $\eta_{\Delta c}$ is neglected). This is an acceptable assumption in the present study, since it is aimed at comparing different membrane/channel arrangements rather than at predicting the stack performance. Thus the electrical current is:

$$I = \langle i\rangle S_{stack} \tag{11}$$

By considering the external circuit, the electrical current and the cell pair voltage are related as

$$I = \frac{n \, V_{cp}}{R_{blank} + R_{ext}} \tag{12}$$

where n is the number of cell pairs; R_{blank} was fixed to 1.0 Ω (from experimental results); and R_{ext} was treated as a variable input parameter. The voltage over the stack, and thus over the external load, is

$$V_{stack} = I \, R_{ext} \tag{13}$$

A cell pair resistance can be calculated as

$$R_{cp} = \frac{OCV_{cp} - V_{cp}}{I} \tag{14}$$

where OCV_{cp} is the open circuit voltage of the cell pair, computed for $R_{ext} \to \infty$ Ω. It should be kept in mind that R_{cp} includes also non-Ohmic resistances and thus depends on the total current I.

The gross power density per cell pair area is

$$GPD = \frac{V_{stack}I}{n\,S_{stack}} \tag{15}$$

The power density consumed for pumping the solutions is

$$PPD = \frac{\Delta p_{CONC}Q_{CONC} + \Delta p_{DIL}Q_{DIL}}{S_{stack}} \tag{16}$$

where Δp_{SOL} and Q_{SOL} are the pressure drop and the volume flow rate in a single concentrate (CONC) or dilute (DIL) channel, calculated as:

$$\Delta p_{SOL} = \frac{(p_{inflow,SOL} - p_{outflow,SOL})}{l}L_{stack} \tag{17}$$

$$Q_{SOL} = u_{SOL}H_{SOL}W_{stack} \tag{18}$$

in which $p_{inflow,SOL}$ and $p_{ouflow,SOL}$ are the pressure at the inflow and outflow periodic boundaries, respectively, l is the length of the periodic domain, u_{SOL} is the superficial velocity of the solution and H_{SOL} is the channel height (inter-membrane distance). Finally, the net power density per cell pair is

$$NPD = GDP - PPD \tag{19}$$

Note that, since fully developed conditions are assumed and all relevant quantities, e.g. GPD, NPD, PPD, are per unit cell pair area, the stack length is irrelevant.

2.3   Computational domain and boundary conditions

A sketch of the domain simulated was shown in Figure 2 along with the sizes and the boundary conditions set. The external boundaries were placed in correspondence of the midplane of the AEM. Periodic conditions were set at the inflow / outflow boundaries, thus simulating fully developed flow and concentration fields. Appropriate source terms were used to account for the large-scale gradients of pressure and concentration, respectively. More precisely, the term **P** added

to the RHS of Eq. (2) was a body force per unit volume representing the large-scale component of the driving pressure gradient along the main flow direction (chosen here to be coincident with the y axis). The term S_i added to the RHS of Eq. (4) was $\dfrac{\dot{M}_i}{V}\dfrac{v}{v_{ave}}$, where $\dot{M}_i$ is the net molar flux of species i exiting the simulated portion of the generic channel, V is its volume, and v, v_{ave} are the local and volume averaged velocity components along the main flow direction. This treatment has been extensively applied to periodic problems in our previous works [21–23,29,31,43] and can be rigorously derived from a decomposition of pressure and concentration into a periodic and a large-scale component. Note that the variables p and c_i obtained by solving Eqs. (2) and (4) now represent periodic components only.

Reducing the computational domain to a small periodic tract of the cell pair allows the spatial resolution to increase while keeping the total number of elements compatible with an acceptable memory requirement and computing time (more details on the mesh are given in section 2.6). However, this implies renouncing to calculating $\eta_{\Delta c}$, but it could be included by coupling the present model with a higher scale model taking into account mass balances from inlet to outlet. For both channels, the superficial velocity (i.e. the velocity calculated by the channel thickness H) was made to vary in the range 0.3-5 cm/s. The bulk concentration (which remains fixed at its initial value in each fluid) was set at 4 M for the concentrate channel and was made to vary in the range 0.005-0.5 M in the dilute channel. The choice of the concentrations was made in order to simulate optimal conditions for the power output, with possible applications in areas where concentrate brines are available or for a closed loop [44,45] where the solutions are regenerated by low grade heat.

The external boundaries were set as periodic with respect to concentration and current density. At the IEM-solution interfaces, the Donnan electrochemical equilibrium conditions were set according to the following formulae [19,46], in which, for simplicity, activity coefficients were set to 1:

$$\phi_{Donnan} = \phi_{\underline{IEM}}^{SOL} - \phi_{IEM}^{SOL} = \frac{RT}{z_{counter}F} \ln \frac{c_{counter,IEM}^{SOL}}{c_{counter,\underline{IEM}}^{SOL}} \tag{20}$$

$$c_{co,\underline{IEM}}^{SOL} - c_{co,IEM}^{SOL} = \left[\frac{1}{2}\left(\sqrt{c_{fix}^2 + 4c_{co,IEM}^{SOL}c_{counter,IEM}^{SOL}} - c_{fix} \right) + ac_{fix} \right] - c_{co,IEM}^{SOL} \tag{21}$$

where ϕ_{Donnan} is the Donnan potential, $\underline{IEM}^{SOL}$ and $\frac{SOL}{IEM}$ indicate IEM side and solution side values, respectively, at the IEM-solution interface, R is the universal gas constant, T is temperature, *IEM* stands for *AEM* or *CEM*, the subscripts *co*, *counter* and *fix* indicate co-ion, counter-ion and fixed charges, respectively. The term *ac_fix* is a correction proposed by Galama *et al.* [41] to account for the presence of minority fixed membrane groups of a charge opposite to that of the membrane or having a strong affinity with the co-ion. On the basis of desorption experiments, the latter authors suggested that these groups represent ~0.1% of the total fixed charge density of the membrane. The term $c_{co,IEM}^{SOL}$ was subtracted from both sides of Eq. (21) merely in order to have them represent the concentration jump across a membrane-solution interface.

The simulations, although leading to a steady state, were actually conducted in transient mode for numerical reasons because this provided a better convergence.

2.4   *Membrane/channel configurations*

Different configurations of the cell pair were simulated as shown in Figure 4. In all cases, the thickness of both concentrate and dilute channels was 270 μm. The side or diameter of the obstacles was slightly more than one half of the channel thickness (150 μm). Of course, empty channels are only an ideal case (as those simulated by Jeong *et al.* [37]), due to the need for mechanically supporting the membranes. The configurations with obstacles in Figure 4 are necessarily only an approximation of actual three-dimensional shapes because in 2-D simulations the obstacles cannot occupy the whole channel height. Similar simplified 2-D shapes have been often simulated in the past in the context of membrane processes, see e.g. Shakaib *et al.* [47] or Tadimeti *et al.* [40]. The

distance between two obstacles on the same side was 600 μm and was chosen as the length of the periodic computational domain.
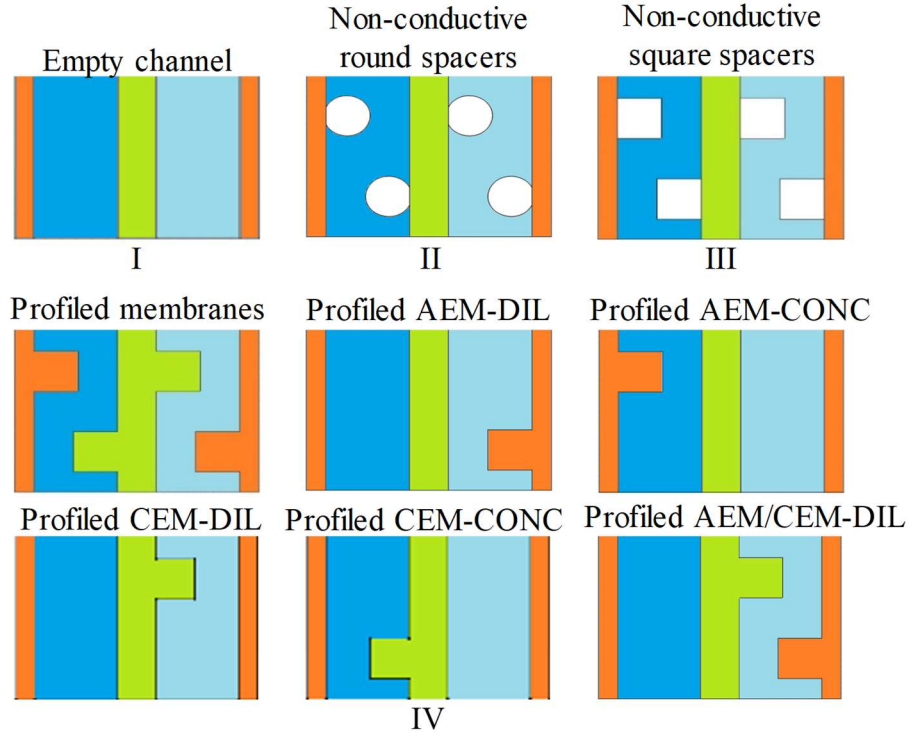

Figure 4. Different membrane/channel configurations simulated: (I) flat membranes and empty channels, (II) flat membranes and non-conductive round spacers placed alternately on both sides of the membranes, (III) flat membranes and non-conductive square spacers placed alternately on both sides of the membranes, (IV) profiled membranes with different arrangements.

2.5 Materials

All the simulations were run at the temperature of 20 °C. NaCl aqueous solutions were simulated. Physical properties within each fluid were set as uniform, as computed at the bulk concentrations. The ions mobility in solution was calculated by the Nernst-Einstein equation

$$m = \frac{D_i}{RT} \tag{22}$$

Membranes were assumed to be homogeneous and isotropic and were simulated as electrolytic solutions with a null flow field. Diffusivity and mobility within the membranes were obtained by model calibration against experimental data. The concentrations of fixed charges in the membranes were assumed to be uniform and equal to 4267 mol/m^3 for the AEM and 4833 mol/m^3 for the CEM on the basis of experimental data on ion exchange capacity and water uptake (FUJIFILM™ membranes). The diffusion coefficient and the mobility of the fixed charges were set to zero.

2.6 Computational details

Hybrid finite element meshes were used (see example in Figure 5). They were composed by quadrilateral elements near the boundaries and triangular elements elsewhere. Grid independence was preliminarily addressed, and a mesh with a total number of elements of ~40,000 was chosen. This mesh exhibits a very good spatial resolution, along with moderate computing times and memory requirements, while finer grids with an order of magnitude of elements more yield only negligibly different results, against a very large increase in computing time and, especially, memory requirements. This feature makes also an accurate simulation of the cell pair from inlet to outlet prohibitive.

The numerical solution of the equation system was structured in two steps: the first step solved the fluid dynamics (*laminar flow* module in COMSOL); the second step solved the electrochemistry (*tertiary current distribution* module), by using the velocity field from the first step. The fully coupled direct solver MUMPS was used for each step.
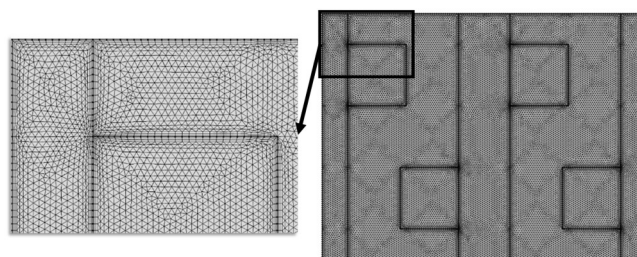

Figure 5. FEM discretization of the computational domain in the case of profiled membranes.

3   Predicted distributions of the main quantities

A large number of simulations was carried out, but, for the sake of brevity, only the main results will be shown and discussed in this paper. Results are reported in this section on the distribution of the main quantities within the cell pair in order to verify the physical consistency of the model predictions. The effects of the various parameters will be discussed in the following section.

3.1   Flow field

Figure 6 shows maps of the velocity module for various geometries simulated. The superficial velocity was assumed equal to 1 cm/s in the two channels. At the very low Reynolds numbers typical of RED channels (< 10) the flow is steady. Within empty channels, the flow is parallel and the velocity exhibits a parabolic profile. When obstacles are present, velocity components perpendicular to the membranes arise, i.e. the flow path becomes tortuous. The larger surface causing friction and the inertial effects cause higher pressure drops; on the other hand, a mixing enhancement is generally obtained, although stagnant regions in the proximity of the obstacles can negatively affect this aspect. Finally, some small differences are caused by the obstacle shape (round vs. square), and the presence of obstacles only on one side of the channel causes larger stagnant regions in the proximity of that side.
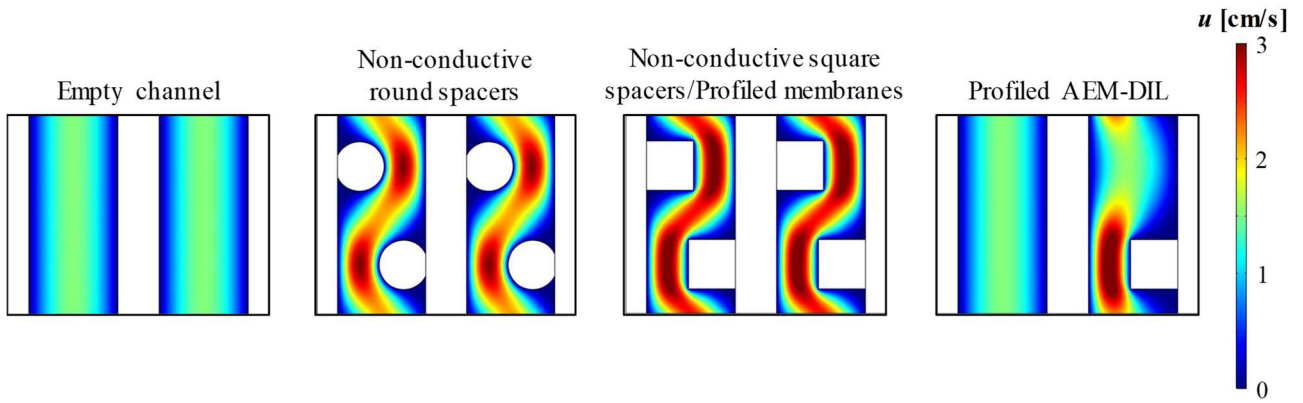
Figure 6. Velocity map for different configurations, at a superficial velocity of 1 cm/s in the two channels.

3.2 Concentration

Transport phenomena of ions involve the whole cell pair, occurring both in the solutions and in the membranes. Figure 7 shows an example of concentration profiles predicted in the case of empty channels. Double layer phenomena are simulated as sudden jumps of concentration at each IEM-solution interface. Because of the electroneutrality condition, in the solutions the concentrations of Na^+ and Cl^- are equal, while in the membranes they differ by a quantity equal to the concentration of the fixed charges. The co-ions concentration inside the membranes is not negligible, due to the high salt concentration in the concentrate solution.

The insets in Figure 7 show also concentration polarization phenomena within the fluid domains. Under open circuit conditions, since the membranes are not perfectly permselective, a diffusive transport takes place, thus generating concentration gradients. Under closed circuit conditions (as in the case shown in Figure 7), a current flows through the stack. In the solutions it is transported in a similar amount by cations and anions (transport numbers ≈ 0.5), while in the membranes it is transported almost exclusively by counter-ions (transport number close to 1). The total flux in the solutions is maintained constant by diffusive fluxes (concentration polarization).
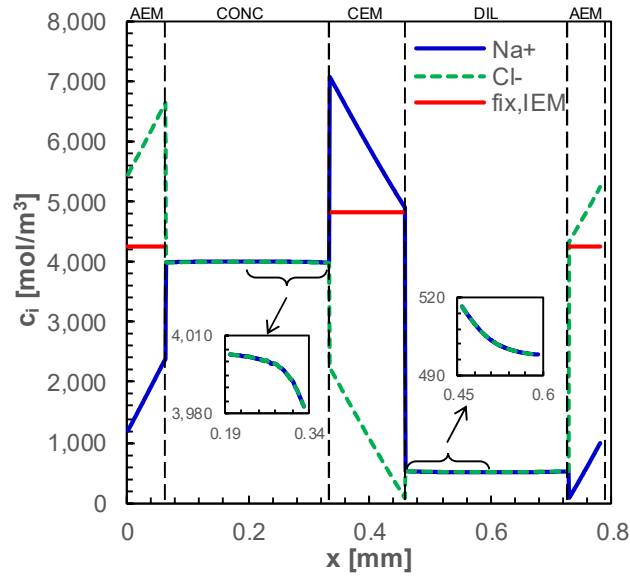
18

Figure 7. Concentration profiles within the cell pair with empty channels, fed by 4M/0.5M solutions at 1 cm/s in the two channels. R_{ext} was set equal to $OCV/I_{short-circuit}$. The values are taken along an arbitrary horizontal line.

3.3 Electrical potential

The Donnan equilibrium for the electrical potential is computed as a sudden jump at each IEM-solution interface, as shown in Figure 8, which reports the potential profiles for different external loads. In particular, the IEM-CONC interfaces are associated with a voltage loss, while the IEM-DIL interfaces are associated with a voltage gain, larger than the IEM-CONC loss.

At open circuit no electrical current circulates, so that there are no voltage losses. The electrical potential is flat also in the membranes since the diffusion coefficients were set at the same values for counter- and co-ions.

At closed circuit, an electrical current flows through the cell pair and the potential exhibits some losses. The largest voltage losses occur in short-circuit conditions, i.e. when the maximum current is circulating. The maximum gross power density is obtained when the stack voltage is approximately equal to $OCV/2$, corresponding to an external resistance equal to the internal one (actually, non-Ohmic phenomena cause a small deviation). The voltage drop is significant within the membranes and, to a lesser extent, within the 0.5M dilute solution. Conversely, the potential

drop within the 4M concentrate solution is negligible, due to the higher electrical conductivity. Note that the large variation of concentration inside the membrane causes a significant variation of conductivity, thus giving the electrical potential profile a curvature.
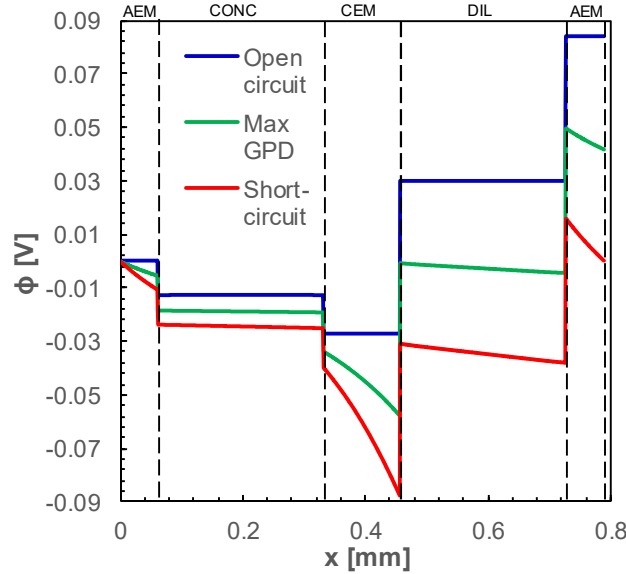

Figure 8. Potential profile within the cell pair with empty channels, fed by 4M/0.5M solutions at 1 cm/s in the two channels, at different external loads. R_{blank} was set equal to zero in order to visualize all the internal losses inside the cell pair. The values are taken along an arbitrary horizontal line.

3.4   Effect of the dilute concentration on the distribution of current density

The performance of a RED stack depends significantly on the electrical conductivity of solutions and membranes. In this regard, it is interesting to consider the current density distribution in complex geometries. Figure 9 shows the current density maps and current lines for a cell pair with profiled membranes fed by $c_{CONC} = 4M$ and $c_{DIL} = 0.01$ (a), 0.05 (b) and 0.1M (c). When the profiles are immersed in a highly conductive solution such as the 4M CONC, they exhibit an almost null current density and are bypassed by the current lines. Conversely, when the profiles are immersed in a less conductive solution such as the 0.01M DIL, plot (a), they are crossed by a significant current density. A concentration of 0.05M, plot (b), is sufficient to confer the dilute solution a conductivity higher than that of the present membranes, and a concentration of 0.1M, plot

(c), makes the current density negligible inside the profiles on the DIL side. Therefore, the features of membranes and solutions significantly affect the usefulness of the profiles for increasing the active area and reducing the stack resistance. Note that the current density distributions in the upstream and downstream obstacle of, say, the dilute channel, are slightly different; this is expected because the two obstacles are parts of two different membranes (AEM and CEM, respectively) characterized by different physical properties and, in particular, electrical conductivities.
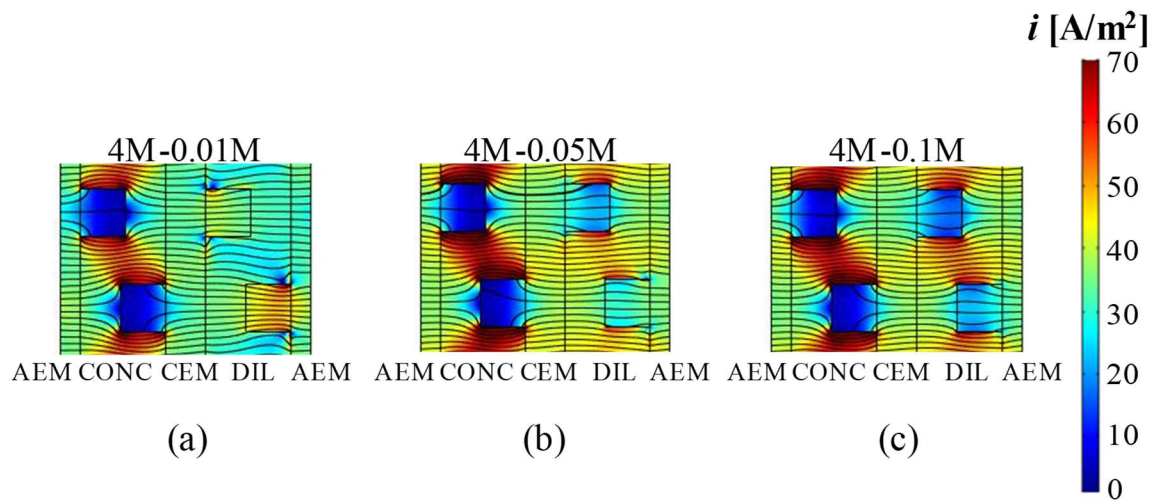

Figure 9. Current density distribution and current lines within the cell pair with profiled membranes, fed by 4M concentrate solution and various dilute solutions at a superficial velocity of 1 cm/s in the two channels. R_{ext} was set equal to $OCV/I_{short-circuit}$.

4   Results validation

For the present two-dimensional simulations, a quantitative validation is possible only by comparison with similarly two-dimensional experiments. We selected from the literature a set of such experiments conducted in electrodialysis channels by Vasil'eva *et al.* [41] using laser interferometry for Reynolds numbers, solution concentrations and geometries similar to those which are the object of the present study.

Comparative results have now been reported in a new section 4 and a new figure 10, which also show and discuss independent COMSOL-based results by Tadimeti *et al.* [40].

Figure 10(a) reports present COMSOL predictions for the concentration distribution in one of the ED configurations studied in [41], characterized by rectangular profiles, 4 mm by 1 mm in size, alternately arranged along the walls of a 2 mm thick channel. The channel was filled by a saline solution with a bulk concentration of 20 mol/m^3 and a Reynolds number (based on superficial velocity and channel thickness) of 5. The channel was subjected to conditions of (direct) electrodialysis with a mean current density of 6.9 A/m^2, corresponding to wall concentrations of about 15 mol/m$^{3.}$ The thick lines indicate the locations in which the concentration is equal to 99% of the bulk concentration; the distance of these lines from the nearest wall was arbitrarily identified by Vasil'eva et al. [41] with the thickness δ_{99} of the diffusion boundary layer. The thin lines orthogonal to the main flow direction are simply markers of locations spaced by 1 mm.

Figure 10(b) reports the thickness δ_{99} relevant to the lower wall as a function of the streamwise coordinate x. Corresponding experimental results by Vasil'eva et al. [41], COMSOL predictions obtained by Tadimeti et al. [40] are shown along with the present COMSOL results. It can be observed that these last are in excellent agreement with the previous experimental and computational results. A comparable agreement was obtained for other configurations in [41].
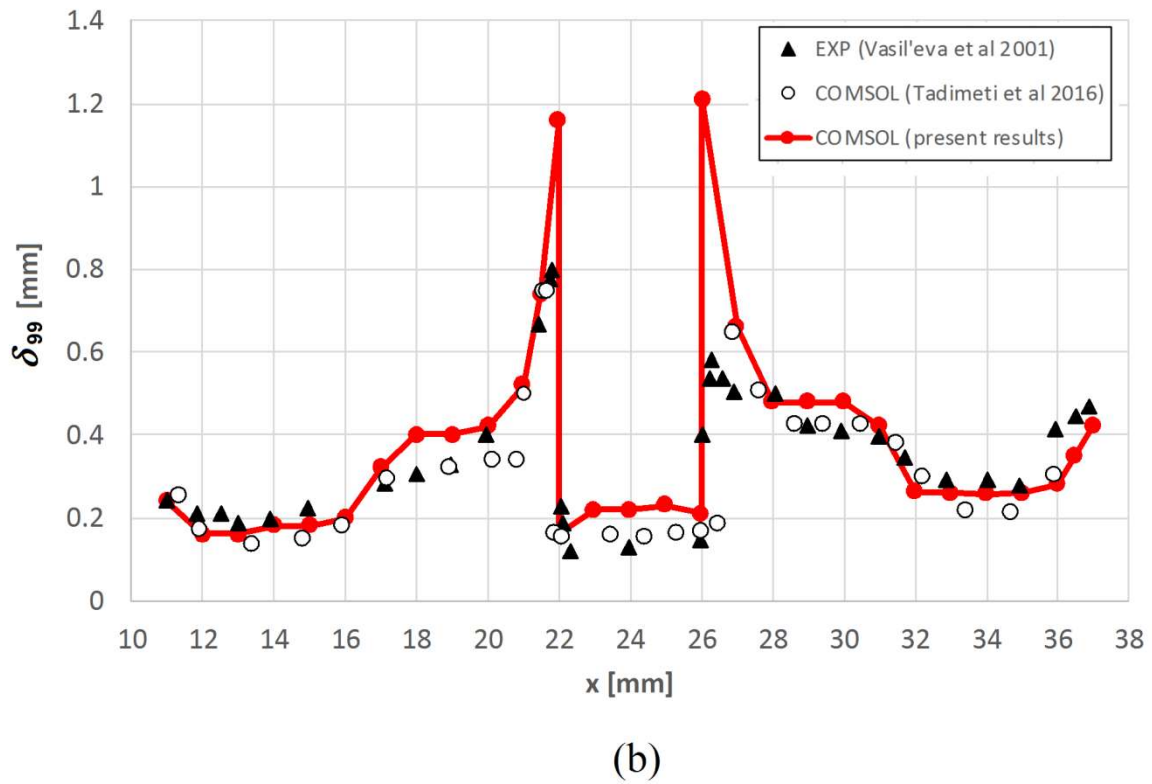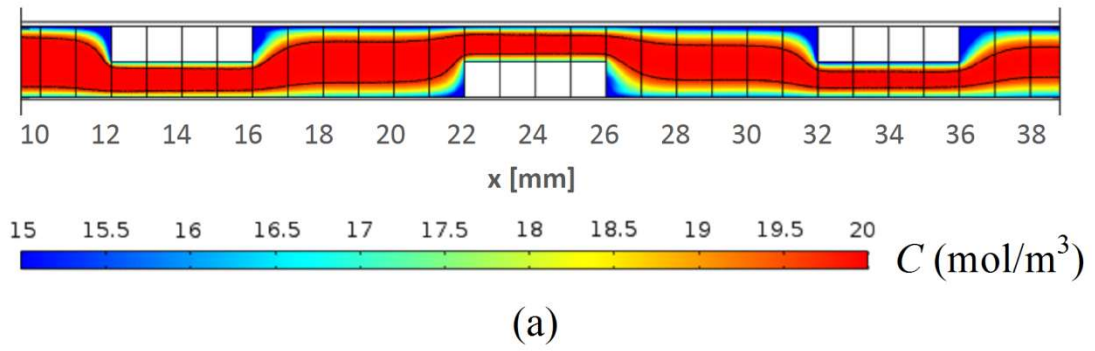
(a)

(b)

Figure 10. Results for electrodialysis in a profiled-membrane channel studied experimentally by Vasil'eva *et al.* [41] (see text for details). (a): predicted concentration distribution; (b) comparison of streamwise profiles of the diffusion boundary layer thickness δ_{99}. Flow from left to right.

5   Sensitivity analysis of the stack performance

This section will describe a sensitivity analysis carried out by maintaining the concentrate at 4M and letting the dilute concentration and the channel configuration vary. The solution velocity was also made to vary in order to find the maximum net power density.

5.1   Gross Power Density

In all cases investigated, the Gross Power Density increases asymptotically towards a maximum as the fluid velocity increases, due to the reduction of the polarization loss η_{BL}. In particular, the increase of GPD is larger when the dilute concentration is lower, as expected. By way of example, Figure 11 reports GPD as a function of the superficial velocity (assumed to be equal in the two channels) for stacks with different membrane/channel configurations, fed by 0.01M/4M (left) and 0.05M/4M (rigth) solutions. For 0.01M dilute solution, left plot, the highest GPD values are obtained with the AEM/CEM-DIL configuration of Figure 4. The same finding emerges also for c_{DIL} = 0.005M (not shown for brevity). On the contrary, in the case of c_{DIL} = 0.05M, right plot, and higher the maximum GPD values were provided by stacks with empty channels. This behaviour highlights that the use of profiles reduces the overall stack Ohmic resistance only in the presence of a dilute solution with very low concentration. Note that different values of GPD are provided by the two configurations profiled AEM-DIL and profiled CEM-DIL, especially at the lower diluate concentration. This is due to the different electrical conductivity of the AEM and CEM membranes, associated in its turn to different values of the fixed charge concentration.
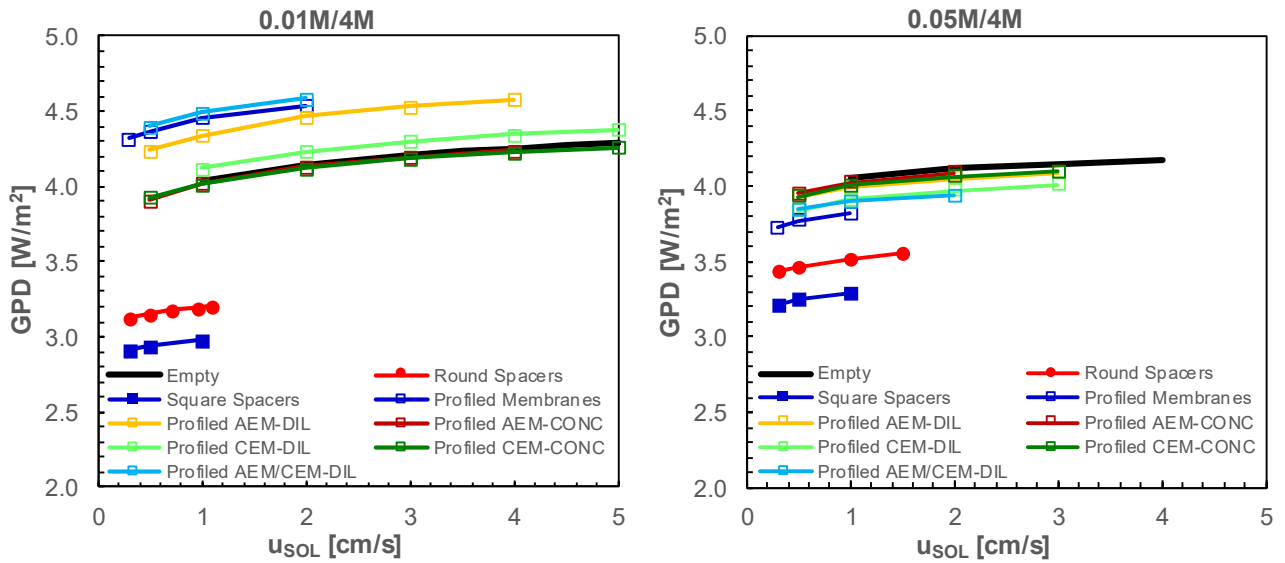
Figure 11. Gross Power Density for stacks (10 cell pairs) with different membrane/channel configurations, fed by 0.01M/4M (left) and 0.05M/4M (rigth) solutions, as a function of the superficial velocity (assumed to be equal in the two channels). R_{ext} was set equal to $OCV/I_{short-circuit}$.

5.2 Pressure drop and Net Power Density

The channel geometry significantly affects the pressure drop. Figure 12 reports the sum of the pressure losses in the concentrate and in the dilute channels per unit stack length for various configurations as a function of the superficial velocity (assumed to be equal in the two channels). One can observe that the presence of obstacles may significantly increase pressure drop. In particular, square obstacles on both sides of both membranes cause the highest values of pressure drop. Round spacers produce a lower hydraulic friction. As the overall number of obstacles per unit length decreases, pressure drop decreases; for example, moving from the AEM/CEM-DIL configuration to the AEM-DIL or CEM-DIL configurations, one can observe an almost twofold reduction of pressure drop. Notably, the pressure drop is higher when profiles are present inside the concentrate channel, due to the higher viscosity and density of the concentrate solution.
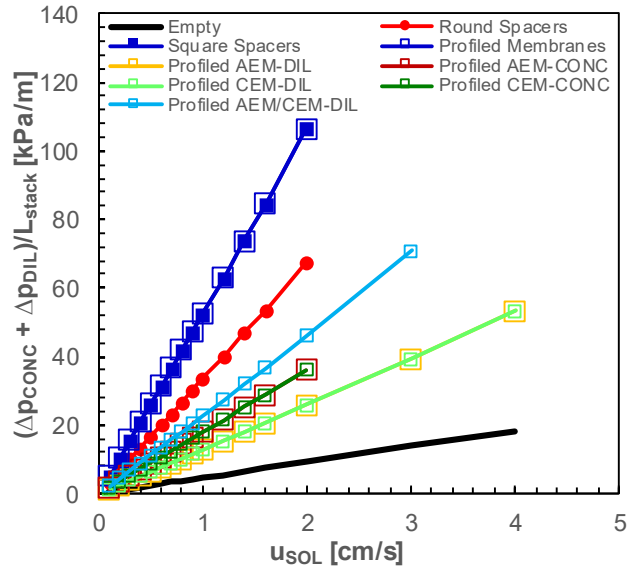
Figure 12. Pressure drop per unit length for different membrane/channel configurations fed by 0.5M/4M solutions, as a function of the superficial velocity (assumed to be equal in the two channels).

Figure 13 reports the Net Power Density for the same cases as in Figure 11. All curves exhibit a maximum as a function of the fluid velocity. As for the case of GPD, at $c_{DIL} \leq 0.01$M the AEM/CEM-DIL configuration yields the highest NPD values (~4.4 W/m^2 for $c_{DIL} = 0.01$M), while at $c_{DIL} \geq 0.05$M it is the empty channel configuration that yields the highest NPD values (~4.1 W/m^2 for $c_{DIL} = 0.05$M).
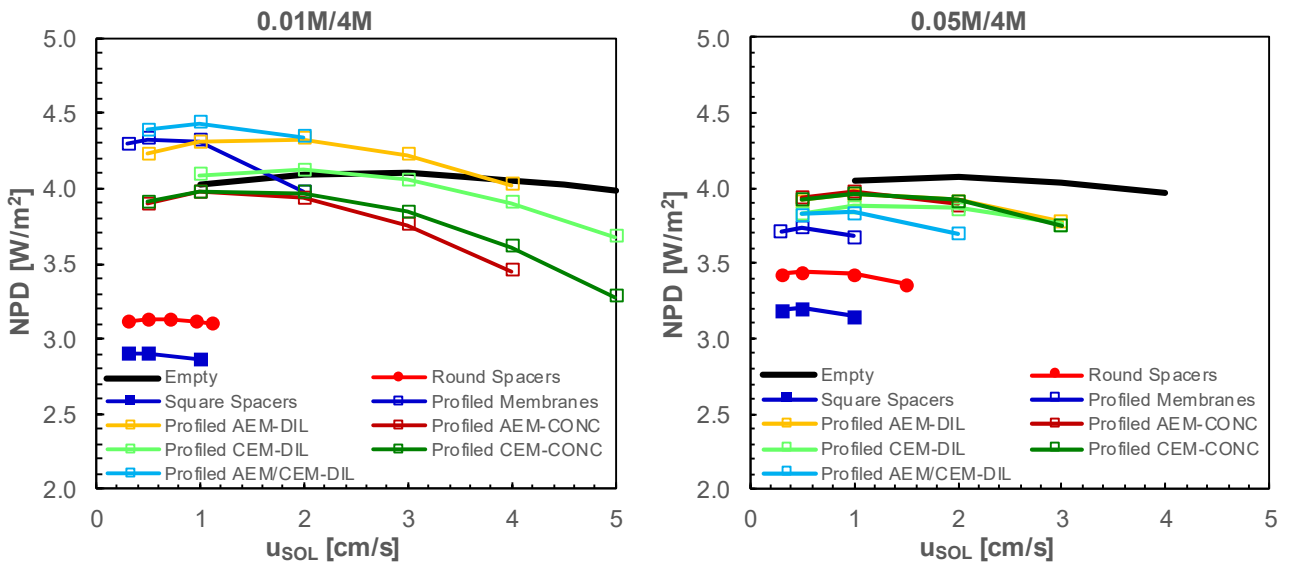
Figure 13. Net Power Density for stacks (10 cell pairs) with different membrane/channel configurations, fed by 0.01M/4M (left) and 0.05M/4M (rigth) solutions, as a function of the superficial velocity (assumed to be equal in the two channels). R_{ext} was set equal to $OCV/I_{short\text{-}circuit}$.

5.3 Optimal conditions (maximum Net Power Density)

This section compares the results obtained for different dilute concentrations and different geometries at the fluid velocity that, for each configuration, maximizes the Net Power Density. In all cases c_{CONC} was kept fixed at 4M.

The values of the cell pair electric resistance under conditions of maximum NPD are shown in Figure 14. This is the total resistance, due to both Ohmic and non-Ohmic phenomena. In order to give an idea of the significance of boundary layer effects, we mention that by using an empty channel 270 μm thick for the dilute solution and the couple 4M/0.01M, the non-Ohmic resistance associated to concentration polarization is ~15% of R_{cp}. The presence of obstacles within the channel enhances mixing, thus reducing the non-Ohmic resistance. In regard to the comparison of non-Ohmic resistance in spacer-filled channels and channels with profiled membranes, our results indicate that differences are negligible provided the geometry and the Reynolds number are the same. The difference in performance in figures 11, 13 and 14 is mainly due to the different Ohmic resistance. Non-conductive spacers cause larger resistances, especially square spacers which occupy a larger volume with respect to round spacers. On the contrary, profiles more conductive than the solution in which they are immersed, e.g. $c_{DIL} \leq 0.01M$, reduce R_{cp}, while empty channels perform better in the case of more conductive solutions. As c_{DIL} increases, R_{cp} decreases, due to the higher conductivity and, to a lesser extent, to the lower boundary layer effect [21]. With a dilute concentration of 0.005M, R_{cp} is about an order of magnitude larger than the resistance with 0.5M.
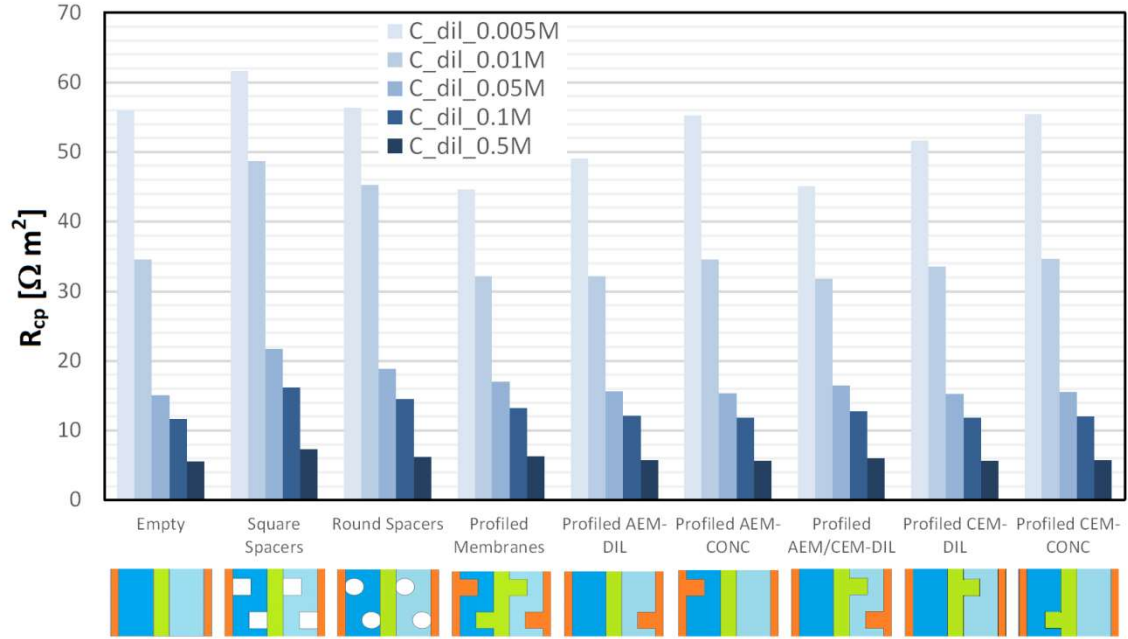
Figure 14. Cell pair areal resistance for different dilute concentrations and membrane/channel configurations, at the superficial velocities (assumed to be equal in the two channels) that maximize the net power density, and with 4M concentrate solution. R_{ext} was set equal to $OCV/I_{short\text{-}circuitt}$.

Besides the overall areal resistance of the cell pair, also the relative importance of Ohmic and non-Ohmic resistances varies as the geometrical configuration, the solution concentrations and the solution velocities vary. For example, Figure 15 reports the relative importance of non-Ohmic resistances (in % of the total cell pair resistance) as a function of the diluate concentration for a 4M concentrate concentration. Results are shown both for square spacers and for profiled membranes.

First, it can be observed that with both configurations the relative importance of non-Ohmic (boundary layer) resistances decreases with the diluate concentration; this is a consequence of the complex concentration-dependence of η_{BL} and polarization coefficients [31].

In regard to the comparative behaviour of the two configurations, it should be remembered that the typical electrical conductivity of the ion exchange membranes is similar to that of a solution of intermediate concentration (~0.01-0.05 M). Therefore, at low diluate concentrations the electrically conducting membrane profiles submerged in the diluate channel reduce its Ohmic

28

resistance with respect to the case of a spacer-filled or empty channel. As a consequence, Ohmic and total resistances are significantly lower for profiled membranes than for spacers, as can be observed in Figure 14, and the relative importance of non-Ohmic losses is rather high (>20%). On the other hand, at diluate concentrations higher than 0.05 M, profiled membranes and non-conductive spacers have a comparable effect in increasing Ohmic (and total) losses, and thus the difference between the two curves in Figure 15 tends to vanish.
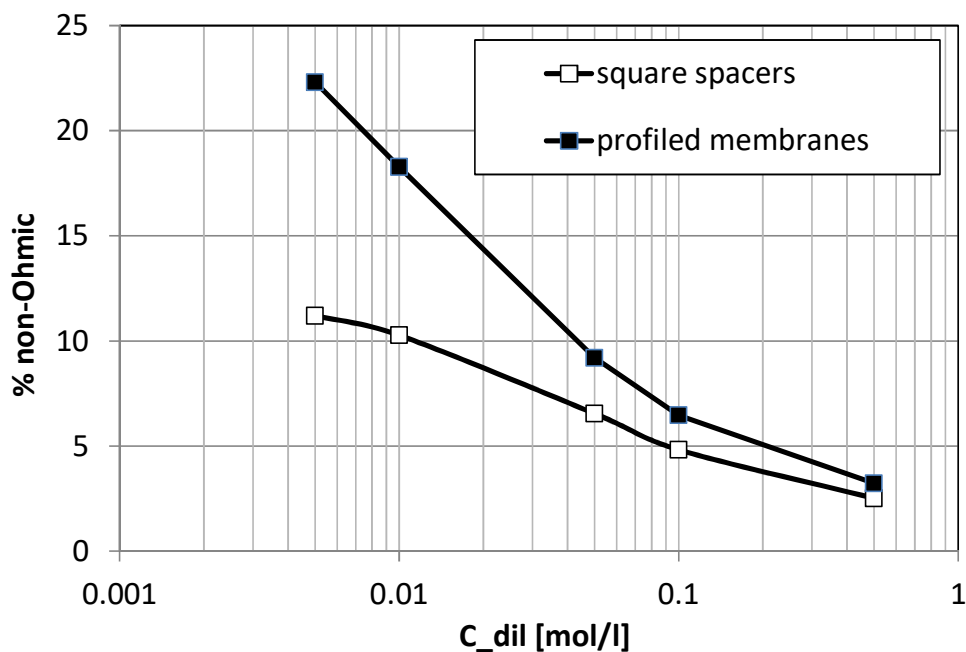

Figure 15. Relative importance of non-Ohmic resistances with respect to the overall cell pair resistance in stacks provided with square spacers and profiled membranes as a function of the diluate concentration and for a 4M concentrate concentration ($u_{DIL} = u_{CONC} = 0.5$ cm/s, conditions of maximum power density).

The Gross Power Density GPD depends on R_{cp} and also on OCV, which, in its turn, is strongly affected by the feeds concentrations. As a consequence, the trend of GPD with c_{DIL} exhibits a maximum. For the present concentration of the concentrate solution (4M), this is obtained at c_{DIL} = 0.01M-0.05M, depending on the geometry. More generally, this optimum c_{DIL} depends on c_{CONC}. Most profiled membranes enhance the process performance with respect to the empty channels for

$c_{DIL} \leq 0.01$M. The features of GPD are reflected into NPD, which is also influenced by the pumping power and, thus, again, by the geometry. Figure 16 reports the maximum Net Power Densities obtained in all the cases simulated. As in the case of GPD, the highest values of NPD are obtained for c_{DIL} = 0.01M-0.05M. Stacks with spacers are characterized by higher R_{cp} and pressure drops, thus leading to lower NPD, especially in the case of the square shape. Profiled membranes increase NPD with respect to the empty channels for $c_{DIL} \leq 0.01$M, yielding the highest NPD ≈ 4.4 W/m^2 with the AEM/CEM-DIL configuration. Stacks with empty channels yield higher NPD than other configurations when $c_{DIL} \geq 0.05$M.
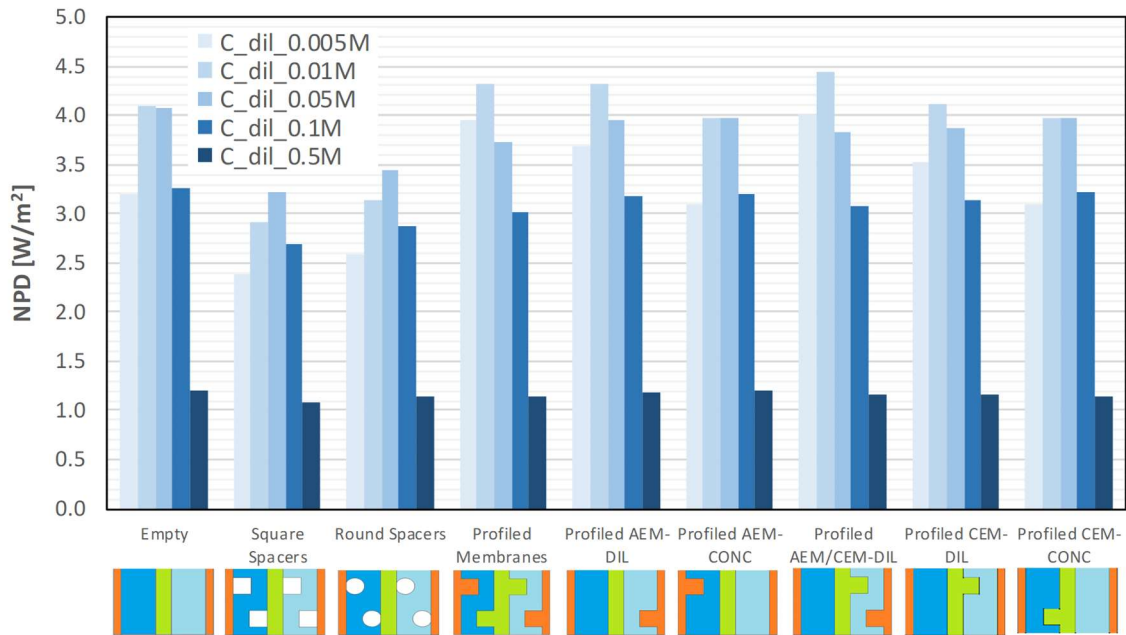

Figure 16. Maximum Net Power Density for different dilute concentrations and membrane/channel configurations, with 4M concentrate solution. R_{ext} was set equal to $OCV/I_{short\text{-}circuit}$.

6   Conclusions

A multi-physical model of RED units was developed. Fluid dynamics, electrochemical mass transport and double layer phenomena were modelled in a two-dimensional periodic domain of a cell pair by the Navier–Stokes equations complemented by the Nernst–Planck approach and the

Donnan exclusion theory. The model is fully predictive and requires only few empirical data as input parameters.

A sensitivity analysis of the stack performance to the stack features and operating conditions, such as membrane/channel configuration, solution concentrations and feed velocities, was conducted. With respect to the ideal case of empty (i.e. spacer-less) channels, cell pairs with non-conductive spacers were characterized by higher electrical resistance and higher pressure drop, and thus by lower net electrical power. The membranes considered in this study were more conductive than solutions with a concentration up to 0.01M, so that profiled membranes reduced the cell electrical resistance with respect to empty channels for c_{DIL} less than this value. This resulted in an increase of gross and net power density at $c_{DIL} \leq 0.01M$, despite the increment in pressure drop. Therefore, the effectiveness of profiled membranes for the active area increase and the stack resistance reduction depends on the stack features and operating conditions, and only in some cases the profiles can actually enhance the stack performance. Of course, manufacturing highly conductive membranes would be important for the process optimization.

The multi-physical model presented possesses great capabilities for treating the complex phenomenology of the RED process. The model is a valid tool to understand the behaviour of RED systems and to investigate the effect of the various operating parameters and stack features. In order to develop a more effective predicting tool, the model should be extended to 3-D geometries and coupled with a higher scale simulation taking into account mass balance from inlet to outlet.

Nomenclature

c_i	Concentration of species i [mol m^{-3}]
D_i	Diffusivity of species i [m^2 s^{-1}]
F	Faraday's constant [C mol^{-1}]
GPD	Gross power density of the stack per cell pair area [W m^{-2}]
I	Electrical current [A]
$\mathbf{i}$	Current density [A m^{-2}]
l	Length of the computational domain [m]
m	Mobility of species i [m^2 V^{-1} s^{-1}]
NPD	Net power density of the stack per cell pair area [W m^{-2}]
$\mathbf{N}_i$	Flux of ions of species i [mol m^{-2} s^{-1}]
OCV	Open circuit voltage over the stack [V]
PPD	Pumping power density of the stack per cell pair area [W m^{-2}]
p	Pressure [Pa]
R_{blank}	Resistance of the electrode compartments [Ω]
R_{cp}	Resistance of the cell pair [Ω]
R_{ext}	Resistance of the external load [Ω]
S_{stack}	Cell pair area (projected) [m^2]
t	Time [s]
$\mathbf{u}$	Velocity vector [m s^{-1}]
V_{stack}	Voltage over the stack [V]
x	Cartesian coordinate along the cross-membrane direction [m]
z_i	Valence of species i [dimensionless]

Greek letters

$\eta_{\Delta c}$	Voltage loss due to the streamwise concentration change in the bulk of the solutions [V]
η_{BL}	Voltage loss due to the concentration polarization in the boundary layers [V]
η_{Ω}	Ohmic voltage loss [V]
μ	Dynamic viscosity [Pa s]
ρ	Density [kg m^{-3}]
ϕ	Electrical potential [V]

Subscripts/superscripts

i	Species i (Na$^+$, Cl$^-$, fixed charges)
CONC	Concentrate
DIL	Dilute
IEM	Ion exchange membrane (anionic or cationic)
SOL	Solution (CONC or DIL)

References

[1]   M. Turek, B. Bandura, Renewable energy by reverse electrodialysis, Desalination. 205 (2007) 67–74. doi:10.1016/j.desal.2006.04.041.

[2]   D. Brogioli, Extracting renewable energy from a salinity difference using a capacitor., Phys. Rev. Lett. 103 (2009) 58501. doi:10.1103/PhysRevLett.103.058501.

[3]   A. Achilli, A.E. Childress, Pressure retarded osmosis: From the vision of Sidney Loeb to the first prototype installation — Review, Desalination. 261 (2010) 205–211. doi:10.1016/j.desal.2010.06.017.

[4]   F. La Mantia, M. Pasta, H.D. Deshazer, B.E. Logan, Y. Cui, Batteries for efficient energy

extraction from a water salinity difference., Nano Lett. 11 (2011) 1810–1813. doi:10.1021/nl200500s.

[5]   R.E. Pattle, Production of Electric Power by mixing Fresh and Salt Water in the Hydroelectric Pile, Nature. 174 (1954) 660–660. doi:10.1038/174660a0.

[6]   A. Cipollina, G. Micale, eds., Sustainable Energy from Salinity Gradients, 1st ed., Woodhead Publishing, Amsterdam, 2016.

[7]   E. Brauns, Salinity gradient power by reverse electrodialysis: effect of model parameters on electrical power output, Desalination. 237 (2009) 378–391. doi:10.1016/j.desal.2008.10.003.

[8]   D.A. Vermaas, M. Saakes, K. Nijmeijer, Enhanced mixing in the diffusive boundary layer for energy generation in reverse electrodialysis, J. Memb. Sci. 453 (2014) 312–319. doi:10.1016/j.memsci.2013.11.005.

[9]   H. Strathmann, Ion-exchange membrane separation processes, first ed., Elsevier, Amsterdam, 2004.

[10]   A. Daniilidis, D.A. Vermaas, R. Herber, K. Nijmeijer, Experimentally obtainable energy from mixing river water, seawater or brines with reverse electrodialysis, Renew. Energy. 64 (2014) 123–131. doi:10.1016/j.renene.2013.11.001.

[11]   M. Tedesco, A. Cipollina, A. Tamburini, I.D.L. Bogle, G. Micale, A simulation tool for analysis and design of reverse electrodialysis using concentrated brines, Chem. Eng. Res. Des. 93 (2015) 441–456. doi:10.1016/j.cherd.2014.05.009.

[12]   J.W. Post, H.V.M. Hamelers, C.J.N. Buisman, Energy recovery from controlled mixing salt and fresh water with a reverse electrodialysis system, Environ. Sci. Technol. 42 (2008) 5785–5790. doi:10.1021/es8004317.

[13]   P. Długołęcki, A. Gambier, K. Nijmeijer, M. Wessling, Practical potential of reverse electrodialysis as process for sustainable energy generation, Environ. Sci. Technol. 43 (2009) 6888–6894. doi:10.1021/es9009635.

[14]   D.A. Vermaas, M. Saakes, K. Nijmeijer, Doubled power density from salinity gradients at

reduced intermembrane distance, Environ. Sci. Technol. 45 (2011) 7089–7095. doi:10.1021/es2012758.

[15]   S. Pawlowski, P. Sistat, J.G. Crespo, S. Velizarov, Mass Transfer in Reverse Electrodialysis: Flow Entrance Effects and Diffusion Boundary Layer Thickness, J. Memb. Sci. 471 (2014) 72–83. doi:10.1016/j.memsci.2014.07.075.

[16]   D.A. Vermaas, M. Saakes, K. Nijmeijer, Power generation using profiled membranes in reverse electrodialysis, J. Memb. Sci. 385–386 (2011) 234–242. doi:10.1016/j.memsci.2011.09.043.

[17]   S. Pawlowski, T. Rijnaarts, M. Saakes, K. Nijmeijer, J.G. Crespo, S. Velizarov, Improved fluid mixing and power density in reverse electrodialysis stacks with chevron-profiled membranes, J. Memb. Sci. 531 (2017) 111–121. doi:10.1016/j.memsci.2017.03.003.

[18]   D.A. Vermaas, E. Guler, M. Saakes, K. Nijmeijer, Theoretical power density from salinity gradients using reverse electrodialysis, Energy Procedia. 20 (2012) 170–184. doi:10.1016/j.egypro.2012.03.018.

[19]   K. Kontturi, M. Lasse, J.A. Manzanares, Ionic Transport Processes in Electrochemistry and Membrane Science, Oxford University Press Inc., New York, 2008. doi:10.1093/acprof:oso/9780199533817.001.0001.

[20]   P. Długołecki, P. Ogonowski, S.J. Metz, M. Saakes, K. Nijmeijer, M. Wessling, On the resistances of membrane, diffusion boundary layer and double layer in ion exchange membrane transport, J. Memb. Sci. 349 (2010) 369–379. doi:10.1016/j.memsci.2009.11.069.

[21]   L. Gurreri, A. Tamburini, A. Cipollina, G. Micale, M. Ciofalo, CFD prediction of concentration polarization phenomena in spacer-filled channels for reverse electrodialysis, J. Memb. Sci. 468 (2014) 133–148. doi:10.1016/j.memsci.2014.05.058.

[22]   L. Gurreri, A. Tamburini, A. Cipollina, G. Micale, M. Ciofalo, Flow and mass transfer in spacer-filled channels for reverse electrodialysis: a CFD parametrical study, J. Memb. Sci. 497 (2016) 300–317. doi:10.1016/j.memsci.2015.09.006.

[23] L. Gurreri, M. Ciofalo, A. Cipollina, A. Tamburini, W. Van Baak, G. Micale, CFD modelling of profiled-membrane channels for reverse electrodialysis, Desalin. Water Treat. 55 (2015) 1–20. doi:10.1080/19443994.2014.940651.

[24] J. Veerman, M. Saakes, S.J. Metz, G.J. Harmsen, Reverse electrodialysis: Performance of a stack with 50 cells on the mixing of sea and river water, J. Memb. Sci. 327 (2009) 136–144. doi:10.1016/j.memsci.2008.11.015.

[25] J. Veerman, M. Saakes, S.J. Metz, G.J. Harmsen, Electrical power from sea and river water by reverse electrodialysis: A first step from the laboratory to a real power plant, Environ. Sci. Technol. 44 (2010) 9207–9212. doi:10.1021/es1009345.

[26] S. Pawlowski, J.G. Crespo, S. Velizarov, Pressure drop in reverse electrodialysis: Experimental and modeling studies for stacks with variable number of cell pairs, J. Memb. Sci. 462 (2014) 96–111. doi:10.1016/j.memsci.2014.03.020.

[27] L. Gurreri, A. Tamburini, A. Cipollina, G. Micale, CFD analysis of the fluid flow behavior in a reverse electrodialysis stack, Desalin. Water Treat. 48 (2012) 390–403. doi:10.1080/19443994.2012.705966.

[28] J. Veerman, M. Saakes, S.J. Metz, G.J. Harmsen, Reverse electrodialysis: A validated process model for design and optimization, Chem. Eng. J. 166 (2011) 256–268. doi:10.1016/j.cej.2010.10.071.

[29] L. Gurreri, A. Tamburini, A. Cipollina, G. Micale, M. Ciofalo, Pressure drop at low reynolds numbers in woven-spacer-filled channels for membrane processes: CFD prediction and experimental validation, Desalin. Water Treat. 61 (2017) 170–182. doi:10.5004/dwt.2016.11279.

[30] Ansys Inc., Ansys-CFX Reference Guide, Release 14.5, (2012).

[31] M. La Cerva, M. Di Liberto, L. Gurreri, A. Tamburini, A. Cipollina, G. Micale, M. Ciofalo, Cupling CFD with simplified 1-D models to predict the performance of reverse electrodialysis stacks, J. Memb. Sci. in press (2017).

[32] S. Pawlowski, V. Geraldes, J.G. Crespo, S. Velizarov, Computational fluid dynamics (CFD) assisted analysis of profiled membranes performance in reverse electrodialysis, J. Memb. Sci. 502 (2016) 179–190. doi:10.1016/j.memsci.2015.11.031.

[33] OpenFOAM, https://openfoam.org.

[34] K.S. Kim, W. Ryoo, M.S. Chun, G.Y. Chung, Simulation of enhanced power generation by reverse electrodialysis stack module in serial configuration, Desalination. 318 (2013) 79–87. doi:doi.org/10.1016/j.desal.2013.03.023.

[35] A.M. Weiner, R.K. McGovern, J.H. Lienhard V, Increasing the power density and reducing the levelized cost of electricity of a reverse electrodialysis stack through blending, Desalination. 369 (2015) 140–148. doi:10.1016/j.desal.2015.04.031.

[36] A.A. Moya, A numerical comparison of optimal load and internal resistances in ion-exchange membrane systems under reverse electrodialysis conditions, Desalination. 392 (2016) 25–33. doi:10.1016/j.desal.2016.04.016.

[37] H.-I. Jeong, H.J. Kim, D.-K. Kim, Numerical analysis of transport phenomena in reverse electrodialysis for system design and optimization, Energy. 68 (2014) 229–237. doi:10.1016/j.energy.2014.03.013.

[38] COMSOL Multiphysics, https://www.comsol.com/.

[39] Z. Zourmand, F. Faridirad, N. Kasiri, T. Mohammadi, Mass transfer modeling of desalination through an electrodialysis cell, Desalination. 359 (2015) 41–51. doi:10.1016/j.desal.2014.12.008.

[40] J.G.D. Tadimeti, V. Kurian, A. Chandra, S. Chattopadhyay, Corrugated membrane surfaces for effective ion transport in electrodialysis, J. Memb. Sci. 499 (2016) 418–428. doi:10.1016/j.memsci.2015.11.001.

[41] V.I. Vasil'eva, V.A. Shaposhnik, O.V. Grigorchuk, Local mass transfer during electrodialysis with ion-exchange membranes and spacers, Russ. J. Electrochem. 37 (2001) 1164–1171.

[42] M. Tedesco, H.V.M. Hamelers, P.M. Biesheuvel, Nernst-Planck transport theory for (reverse) electrodialysis: I. Effect of co-ion transport through the membranes, J. Memb. Sci. 510 (2016) 370–381. doi:10.1016/j.memsci.2016.03.012.

[43] A. Tamburini, G. La Barbera, A. Cipollina, M. Ciofalo, G. Micale, CFD simulation of channels for direct and reverse electrodialysis, Desalin. Water Treat. 48 (2012) 370–389. doi:10.1080/19443994.2012.705084.

[44] M. Reali, Closed cycle osmotic power plants for electric power production, Energy. 5 (1980) 325–329. doi:10.1016/0360-5442(80)90033-X.

[45] W. Huang, W.S. Walker, Y. Kim, Junction potentials in thermolytic reverse electrodialysis, Desalination. 369 (2015) 149–155. doi:doi.org/10.1016/j.desal.2015.05.005.

[46] A.H. Galama, J.W. Post, M.A. Cohen Stuart, P.M. Biesheuvel, Validity of the Boltzmann equation to describe Donnan equilibrium at the membrane–solution interface, J. Memb. Sci. 442 (2013) 131–139. doi:10.1016/j.memsci.2013.04.022.

[47] M. Shakaib, S.M.F. Hasani, I. Ahmed, R.M. Yunus, A CFD study on the effect of spacer orientation on temperature polarization in membrane distillation modules, Desalination. 284 (2012) 332–340. doi:10.1016/j.desal.2011.09.020.